Wet-spun Ni, N-Codoped Macroporous Carbon Fibers for Efficient CO_2 Electroreduction and Zn-CO_2 Batteries

1. Experimental Section

1.1 Materials

Nickel(II) acetylacetonate ($Ni(acac)_2$, 95%), melamine (MA, ≥99%), cyanuric acid (CA, ≥98%), polyacrylonitrile (PAN, Mw=150000), and potassium bicarbonate ($KHCO_3$, ≥99.5%) were all purchased from Macklin Chemistry Co. Ltd. Dimethyl sulfoxide (DMSO, ≥99%), N, N-Dimethylformamide (DMF, AR), and Ethylene glycol (EG, ≥99.5%) were all purchased from Tianjin Fuyu Fine Chemical Co. Ltd.

1.2. Synthesis of MCA nanosphere.

MCA nanosphere is prepared by a simple room temperature self-assembly method. Typically, 10 mmol of melamine (1.26 g) and 10 mmol of cyanuric acid (1.29 g) were dissolved in 100 mL of dry mixed solvent (V_{DMSO} : V_{EG} =1:3), respectively. Then, the melamine solution is poured into the cyanuric acid solution stirring for 1 h, and left undisturbed at room temperature for 4 h. The precipitate was centrifugated, washed with ethanol 3 times, and dried at 60°C overnight.

1.3. Synthesis of Ni-NC-x and NC

In a typical synthesis, MCA nanosphere (0.6 g) and $Ni(acac)_2$ (10 mg) were dispersed into 5 mL DMF and ultrasonic for 1 h. Subsequently, 200 mg of PAN was added to the solutions and stirred at 80 ℃ for 3 h. The obtained MCA/Ni^{2+}/PAN solution was used as a precursor for the wet spinning of composite fibers (**Figure. S1**). During the spinning process, the precursor solution was directly transported to deionized water with a flow rate of 0.2 mL·min^{-1} by a syringe pump. The collected fibers were washed with ethanol 2 times and dried at 60°C for 2 h. Then, the obtained fibers were pre-oxidized in an air atmosphere at 230°C for 1 h with a heating rate of 1°C·min^{-1} and then carbonized at 900 °C for 2 h with a heating rate of 5 °C·min^{-1} in N_2. The resultant Ni, N-codoped carbon macroporous fibers were denoted as Ni-NC-10. The amounts of $Ni(acac)_2$ (1, 10, and 100 mg) were regulated and these obtained

samples were labeled as Ni-NMCF-x (x represents the amount of $Ni(acac)_2$). The pyrolysis temperatures (800 and 1000 ℃) were controlled and these obtained samples were labeled as Ni-NMCF-10 (T) (T represents the calcination temperature). The Ni-free catalyst (NMCF) was also synthesized by a similar method without the addition of the $Ni(acac)_2$.

1.4 Synthesis of Ni NPs-NC

In a typical synthesis, MCA nanosphere (0.6 g) and $Ni(acac)_2$ (100 mg) were dispersed into 5 ml DMF and ultrasonic for 1 h. Subsequently, 200 mg of PAN was added to the solutions and stirred at 80 ℃ for 3 h. After pouring on a plastic film and drying at 80 ℃ to form a thin membrane. Then, the thin membrane was pre-oxidized in an air atmosphere at 230 °C for 1 h with a heating rate of $1°C \cdot min^{-1}$ and then carbonized at 900 °C for 2 h with a heating rate of 5 $°C \cdot min^{-1}$ in N_2. The resultant Ni nanoparticles and N-doped macroporous carbon were denoted as Ni NPs-NMC.

1.5. Characterizations

The crystal structure of the as-prepared electrocatalysts was verified by XRD (Bruker-D8, Cu Kα radiation). The morphologies and particle sizes of the catalysts were characterized by scanning electron microscopy (SEM, Hitachi S-4800) and transmission electron microscope (TEM, FEI Talos F200S). The chemical state of the electrocatalysts was examined by X-ray photoelectron spectroscopy (XPS, KRATOS AXIS Ultra DLD) and the spectra were calibrated using C1s peak at 284.6 eV. N_2 adsorption-desorption was conducted at 77 K using the ASAP 2020 instrument with degassing samples (200 ℃ for 2 h for the porous structure and surface area characterization. Contact angle measurements were performed on a Biolin Scientific contact angle analyzer.

1.6. Preparation of working electrodes

To prepare the working electrode, 5 mg catalysts and 20 μL Nafion solution (5 wt. %) were dispersed into 980 μL of ethanol solution and sonicated for at least 30 min to generate a well-dispersed catalysts ink. 12 μL ink was loaded onto an L-type glassy carbon electrode with a 5 mm diameter, giving a catalyst loading of 0.3 $mg \cdot cm^{-2}$.

1.7. Electrochemical measurements

Electrochemical measurements were performed in a gas-tight H-type cell, separated by a proton exchange membrane (Nafion 117). The electrolyte in the cathode and anode chamber was all 25 mL 0.5 M $KHCO_3$ solution. The L-type glassy carbon was used as the working electrode. Ag/AgCl and Pt plate (1.0 cm×1.0 cm) were used as reference and counter electrodes. CHI660E (CH, China) was used as an electrochemical workstation. High-purity CO_2 (99.999%) with a flow rate of 20 sccm was continuously purged into electrolytes for at least 30 min to make CO_2 saturated. All potentials in the H-cell test were measured against the reference electrode and converted to the RHE reference using E (vs. RHE) =E (vs. Ag/AgCl) +0.198+0.0591×pH, and the pH of CO_2 and Ar-saturated 0.5 M $KHCO_3$ solution is 7.2 and 8.4, respectively. Before testing the activity, 20 cycles of cyclic voltammetry (CV) were used to activate the catalysts and make the catalyst's performance reach the best. Linear sweep voltammetry (LSV) was performed in Ar-saturated and CO_2-saturated 0.5 M $KHCO_3$ solution with a scan rate of 10 $mV \cdot s^{-1}$ and CO_2 electroreduction performance of catalysts at different potentials was evaluated by using chronoamperometry (CA) for 30 min at each potential. Stirring (1000 rpm) was used to accelerate the mass transfer of the cathode chamber during the measurement. The electrochemical impedance spectroscopies (EIS) were recorded at -0.5 V in CO_2-saturated 0.5 M $KHCO_3$ electrolyte under static conditions, the perturbation amplitude was 5 mV, and the frequency range was from 100 KHz to 100 mHz. The gas products were analyzed by an online gas chromatography (GC) system (SCION, 456C) using high-purity Ar (99.999%) as the carrier gas. The liquid products (500 μL electrolyte mixed with 100 μL D_2O and 100 μL dimethyl sulfoxide solution (6 $mmol \cdot L^{-1}$)) were analyzed by Bruker AV400 NMR spectrometer.

The Faradaic efficiency (FE) of the products was calculated as follows:

$$FE = {Q_{product}}/{Q_{total}} = {NZF}/{Q_{total}}$$

where N is the moles of product. Z stands for the number of transfer electrons, which was 2 for H_2 and CO, respectively. F is the Faradaic constant (96485 $C \cdot mol^{-1}$); Q_{total}

represents the total quantity of electric charge during the whole CO_2 reduction process.

1.8. Flow cell test

In the flow cell tests, the catalyst-coated gas diffusion electrodes (GDEs), Hg/HgO, and Pt sheets (0.5 cm × 2 cm) were employed as the working electrode, reference electrode, and counter electrode, respectively. The cathodic and anodic chambers were divided with an anion exchange membrane (Fumasep, FAA-3-PK-130) and then these three components were positioned and clamped together using polytetrafluoroethylene (PTFE) spacers. 1 M KOH (pH=14) solution was employed electrolytes. CO_2 flow was controlled at 20 $mL \cdot min^{-1}$ by using a mass flow controller, and the mass loading of the catalyst was 1 $mg \cdot cm^{-2}$. The electrolyte flow was kept at 5 $mL \cdot min^{-1}$ with peristaltic pumps (BT100M). All measured potentials were converted to a reversible hydrogen electrode (RHE) without iR compensation..

1.9. Zn-CO_2 battery measurement

The Zn-CO_2 battery was constructed by the flow cell and the two compartments were separated by a bipolar membrane. The cathodic and anodic electrolytes were 1 M $KHCO_3$ and 6 M KOH. The flow rate of CO_2 was controlled at 20 sccm during the testing. A zinc plate with a geometric area of 6.15 cm^2 was applied as an anode after mechanical polishing, while a gas diffusion electrode with catalysts (0.6 $mg \cdot cm^{-2}$) was used as a cathode.

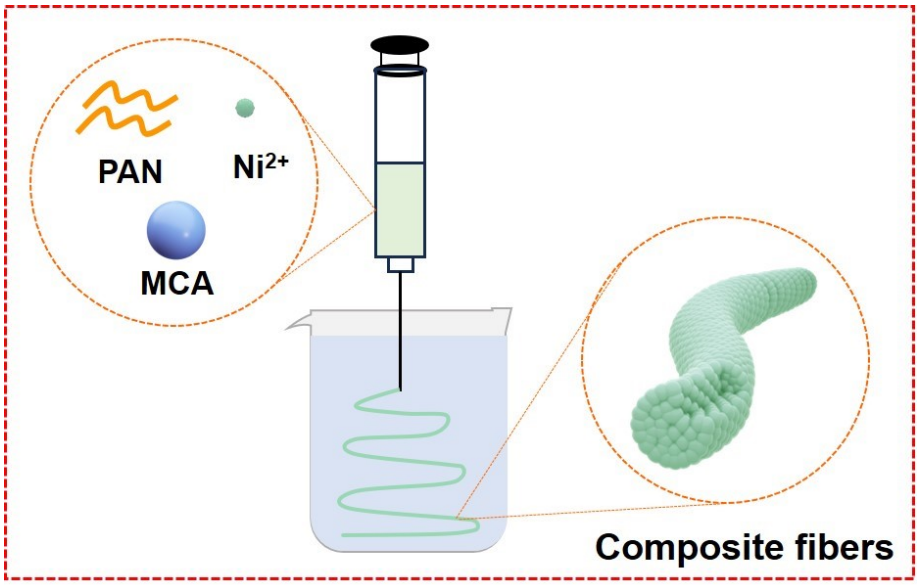

Figure S1. Schematic diagram of the synthesis fiber process.

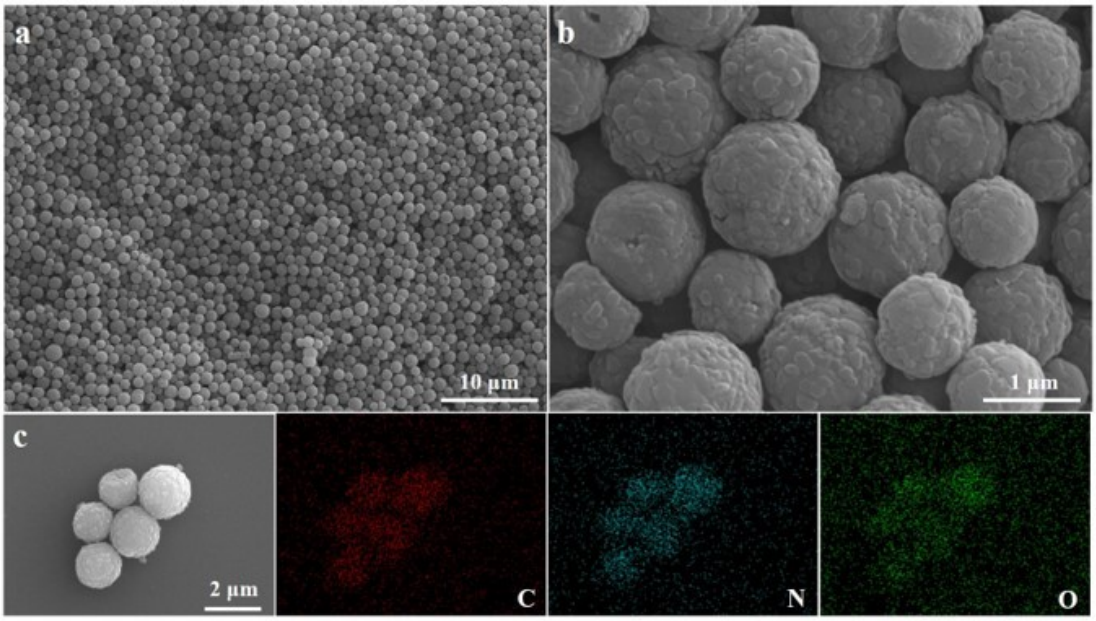

Figure S2. a, b) SEM images, and **c)** Elemental mapping images of MCA spheres.

Figure S3. The digital image of fiber prepared by wet spinning.

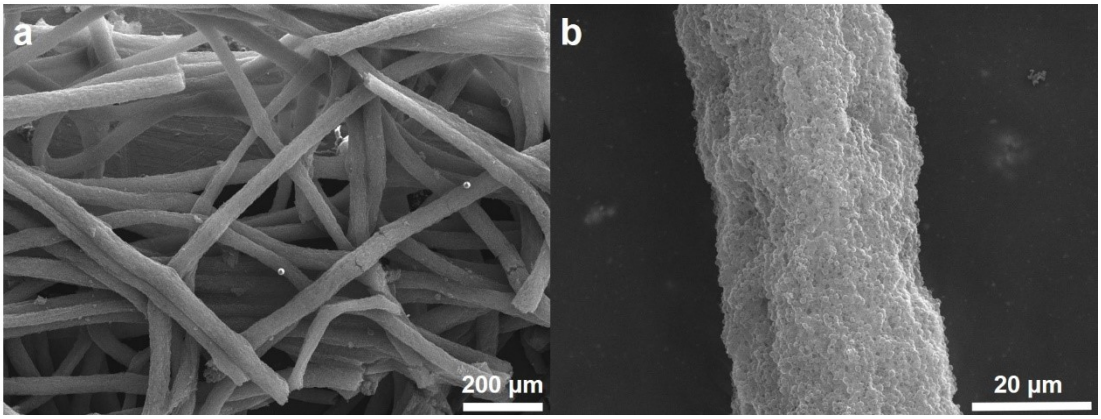

Figure S4. SEM images of Ni-NMCF-10.

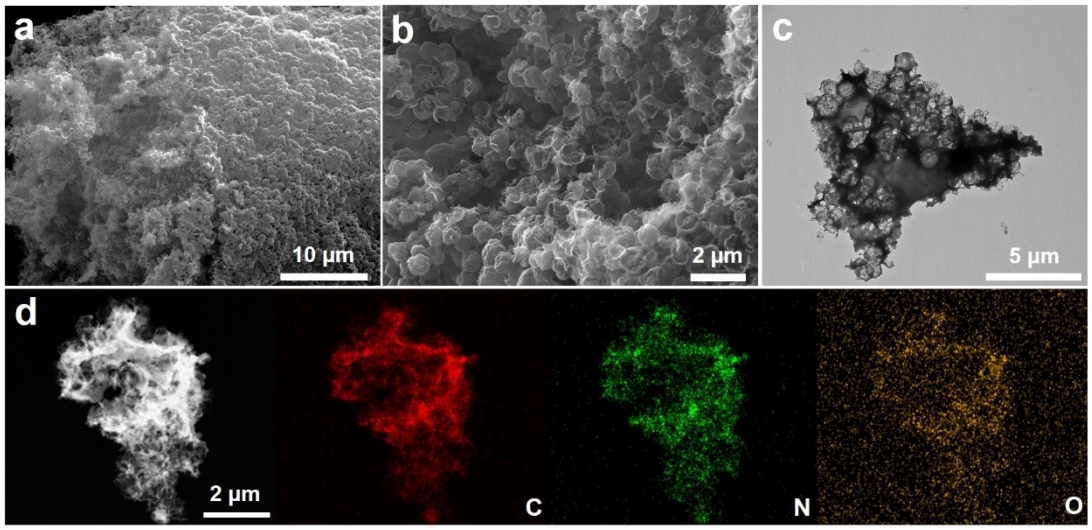

Figure S5. a, b) SEM images, **c)** TEM images, and **d)** EDX elemental mapping images of NMCF.

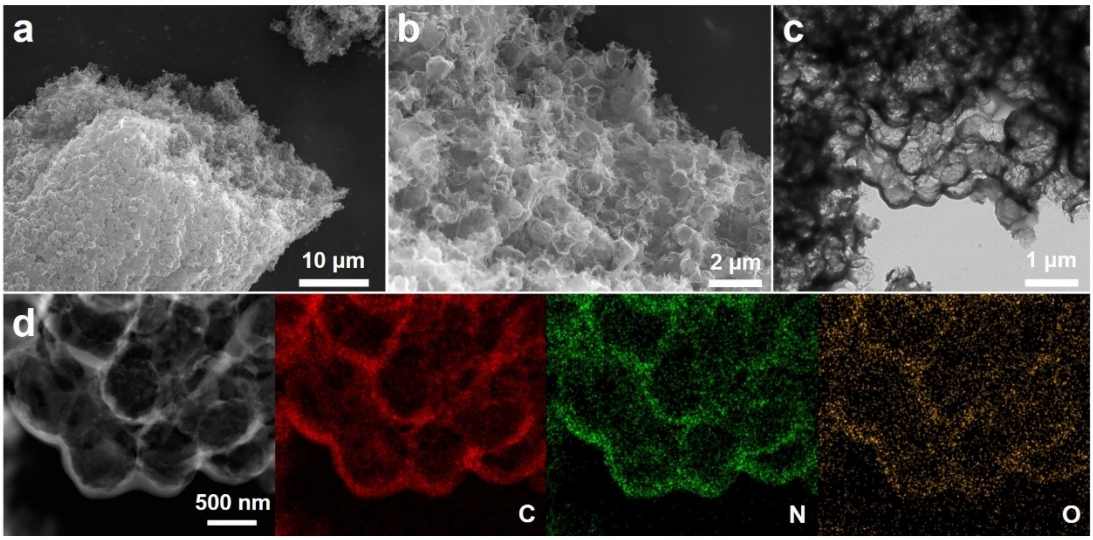

Figure S6. a, b) SEM images, **c)** TEM images, and **d)** EDX elemental mapping images of Ni-NMCF-1.

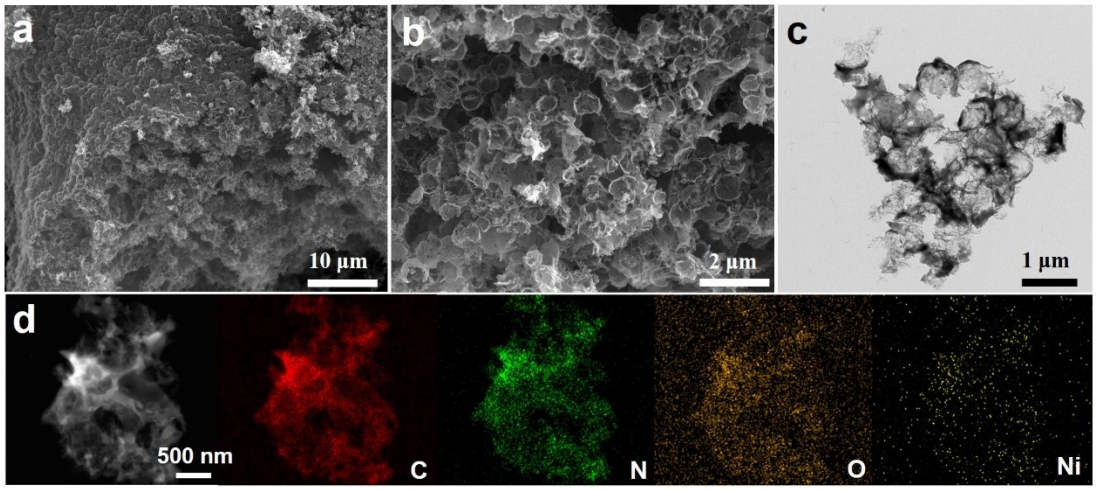

Figure S7. a, b) SEM images, **c)** TEM images, and **d)** EDX elemental mapping images of Ni-NMCF-100.

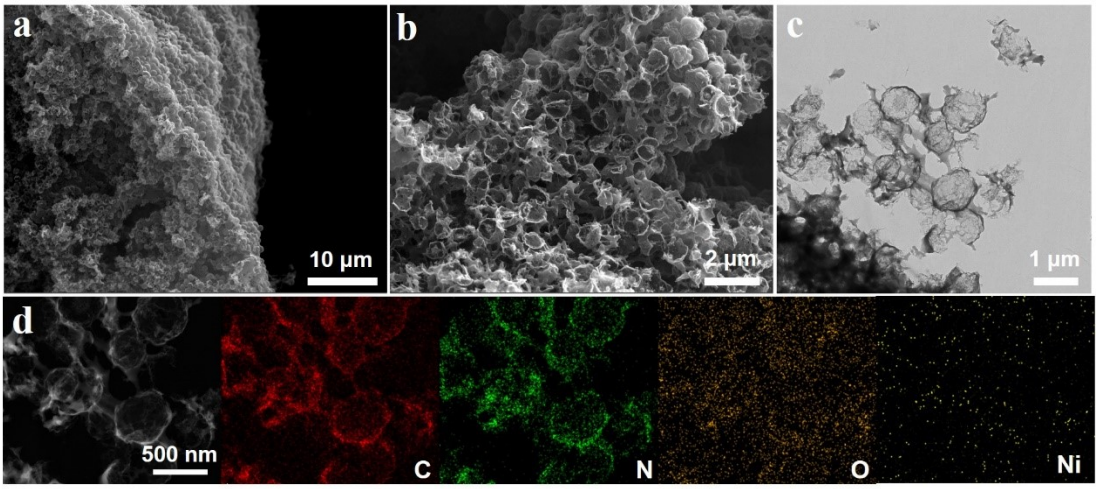

Figure S8. a, b) SEM images, **c)** TEM images, and **d)** EDX elemental mapping images of Ni-NMCF-10 (800°C).

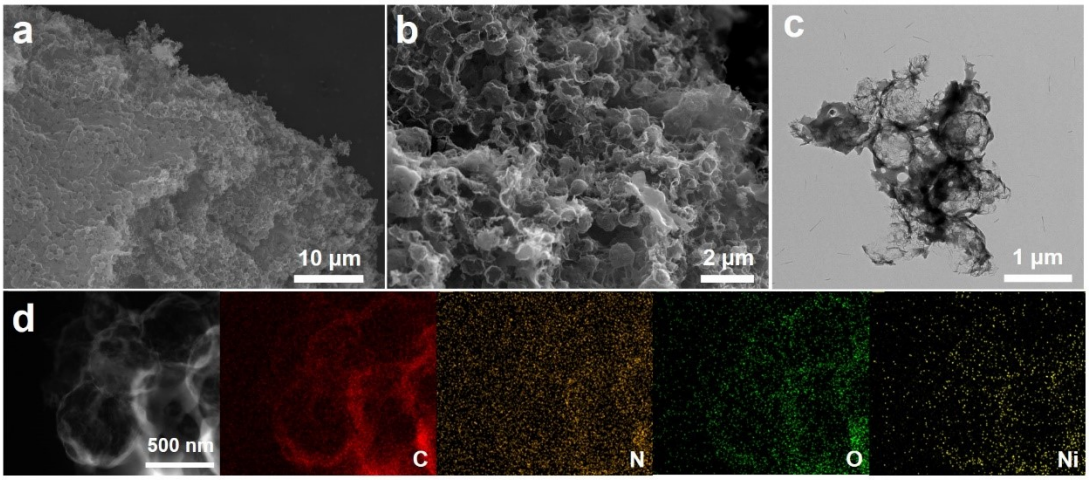

Figure S9. a, b) SEM images, **c)** TEM images, and **d)** EDX elemental mapping images of Ni-NMCF-10 (1000℃).

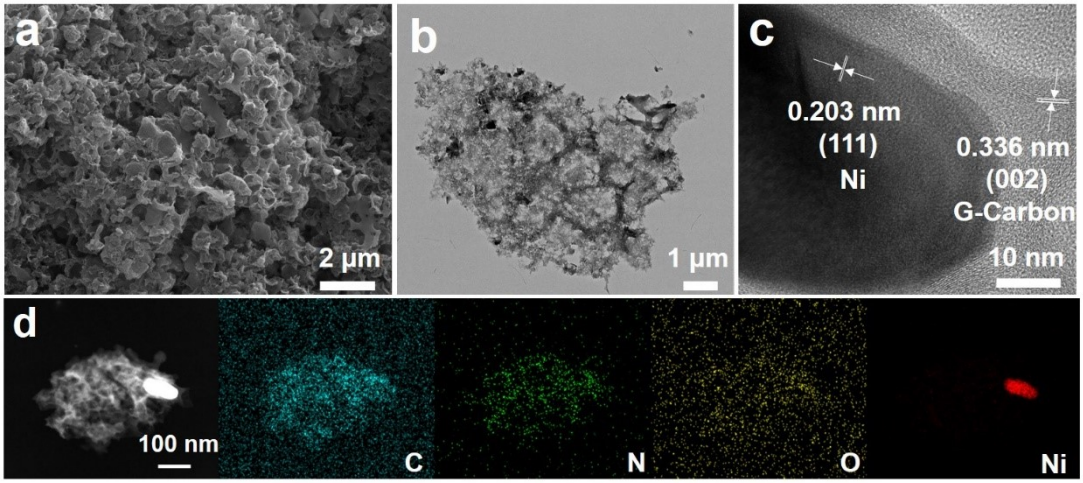

Figure S10. a, b) SEM images, **c)** TEM images, and **d)** EDX elemental mapping images of Ni NPs-NMC.

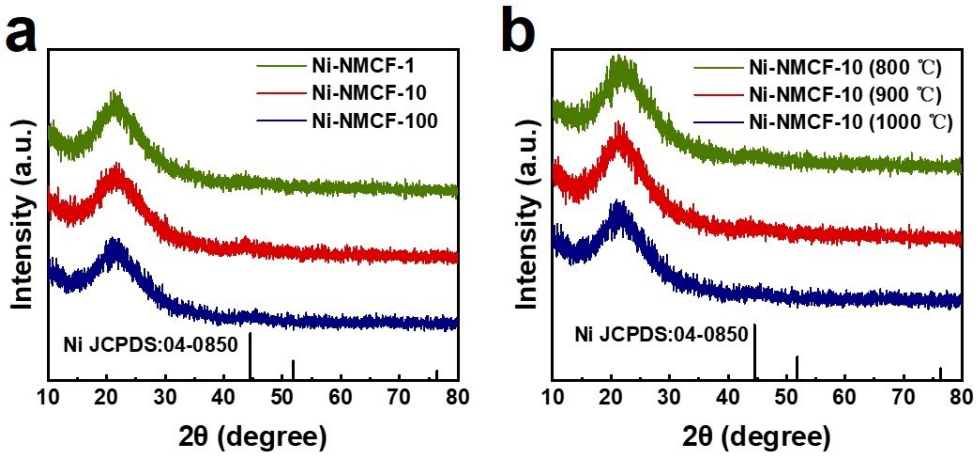

Figure S11. XRD patterns of **a)** Ni-NMCF-x and **b)** Ni-NMCF-10 (T).

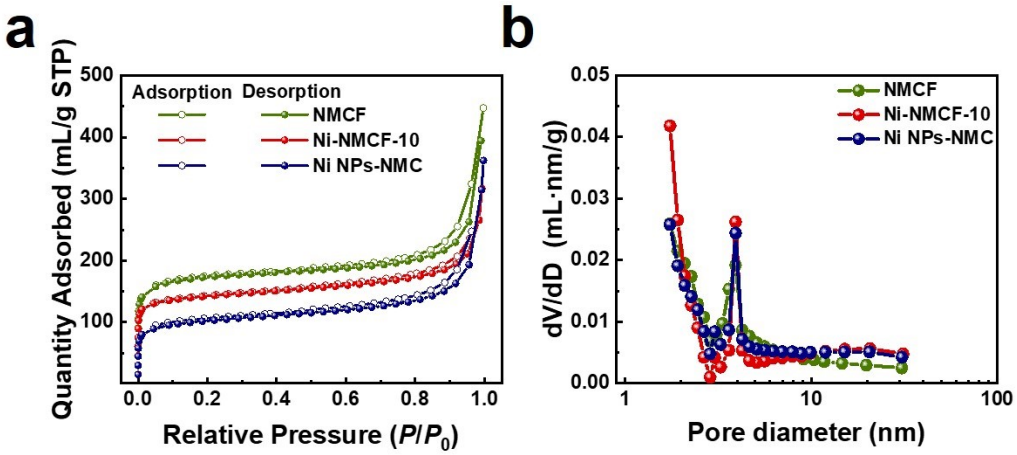

Figure S12. a) N_2 adsorption-desorption isotherms and **b)** the corresponding BJH pore size distribution curves of NMFC, Ni-NMFC-10, and Ni NPs-NMC samples.

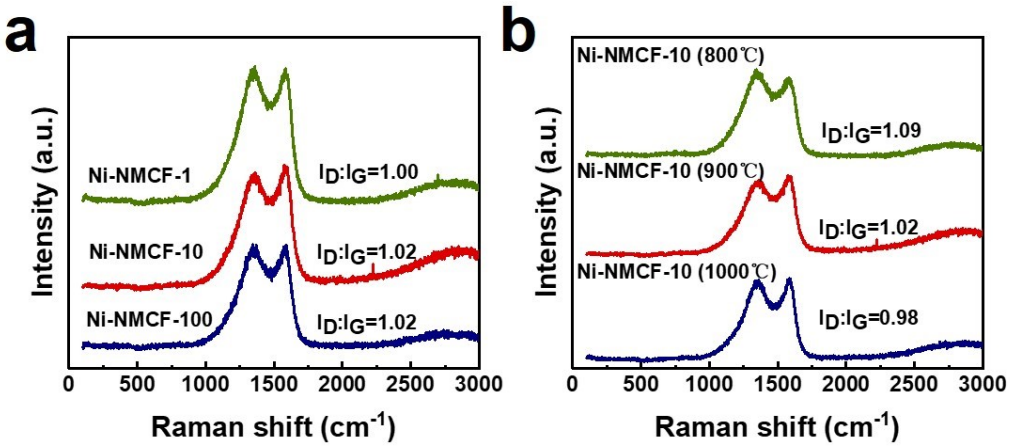

Figure S13. Raman spectra of **a)** Ni-NMCF-x and **b)** Ni-NMCF-10 (T).

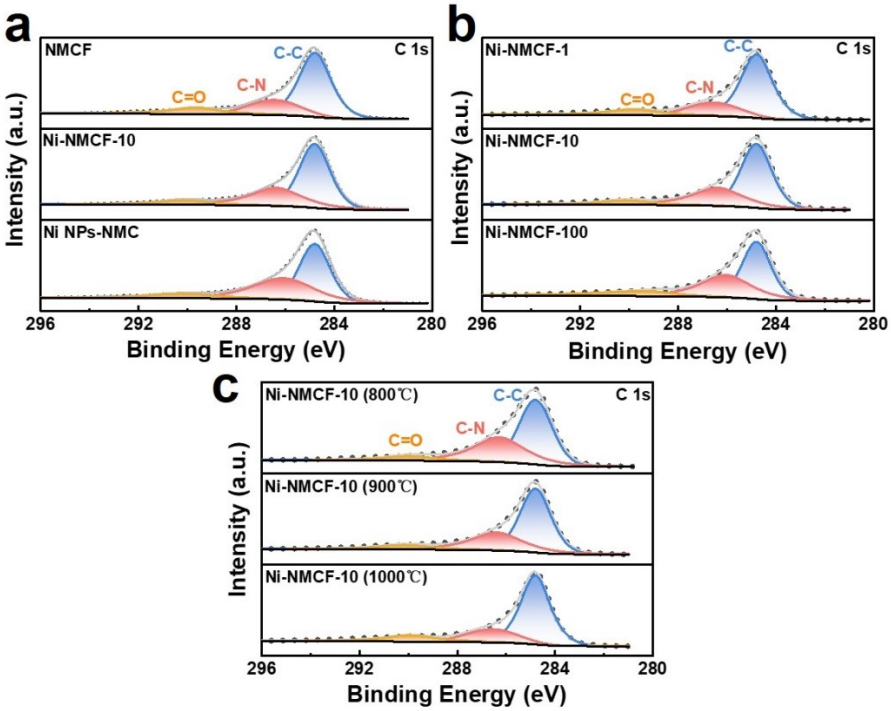

Figure S14. C 1s spectra of the prepared catalysts.

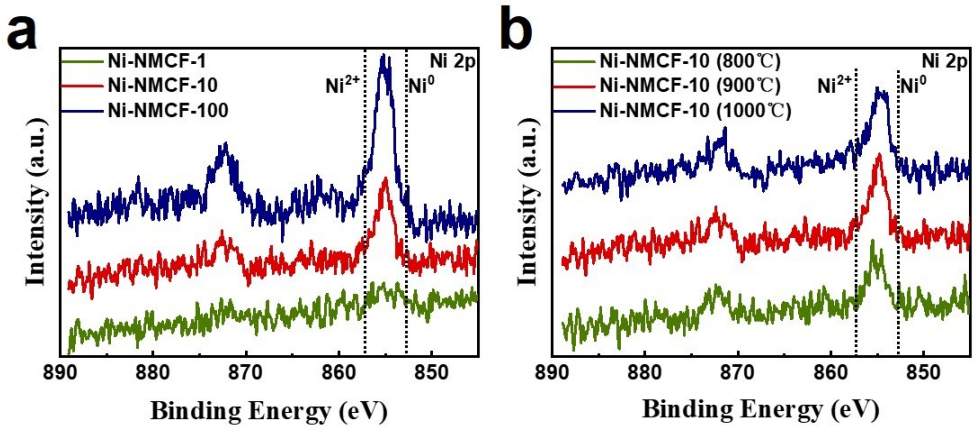

Figure S15. Ni 2p XPS spectra of **a)** Ni-NMCF-x and **b)** Ni-NMCF-10 (T).

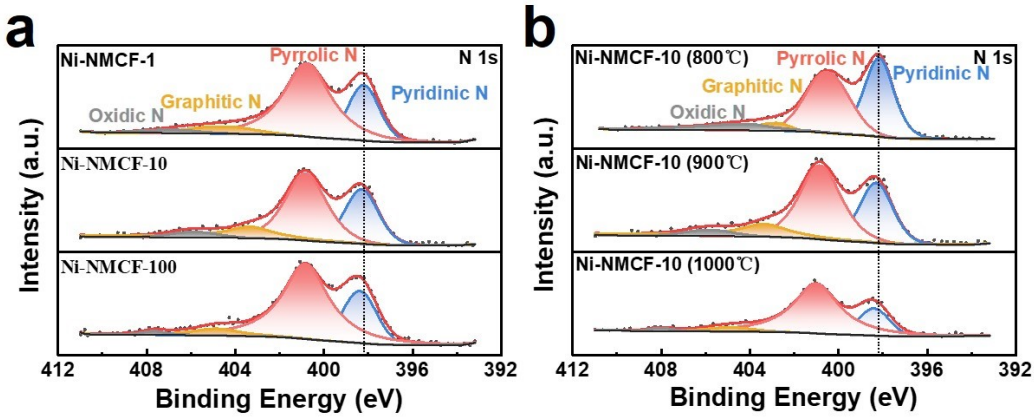

Figure S16. N 1s XPS spectra of **a)** Ni-NMCF-x and **b)** Ni-NMCF-10 (T).

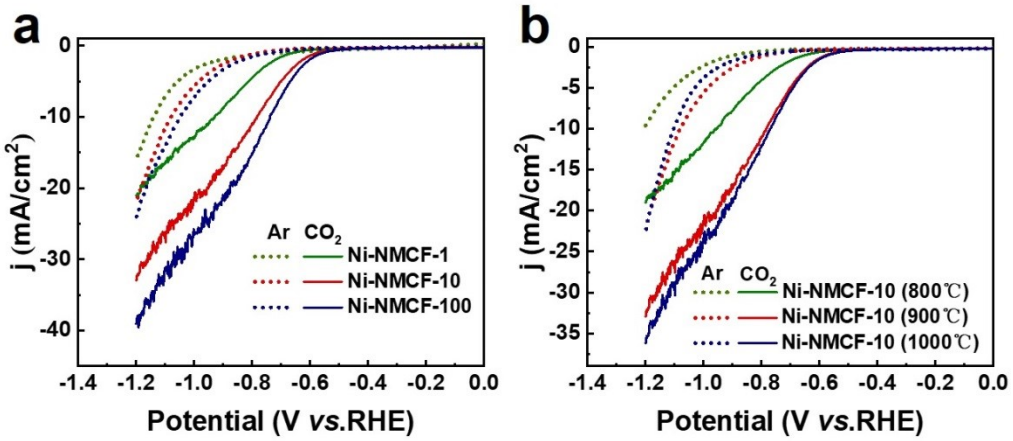

Figure S17. LSV curves in Ar/CO_2-saturated 0.5 M $KHCO_3$ electrolyte at a scan rate of 10 mV·s^{-1} for the **a)** Ni-NMCF-x and **b)** Ni-NMCF-10 (T).

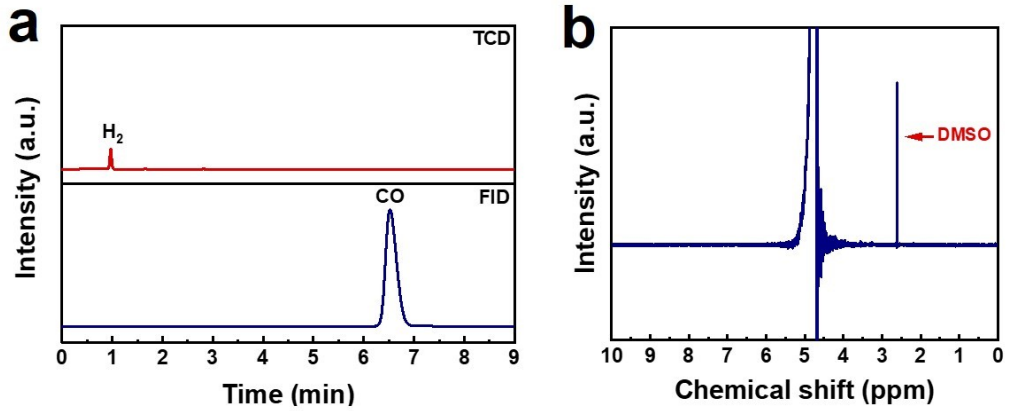

Figure S18. a) Gas chromatography (GC) analysis of gas products (CO, H_2) released by the Ni-NMCF-10 catalyst at -0.8 V. **b)** ^{1}H-NMR spectrum of the Ni-NMCF-10 catalyst for liquid products of accumulated electrolyte at -0.8 V.

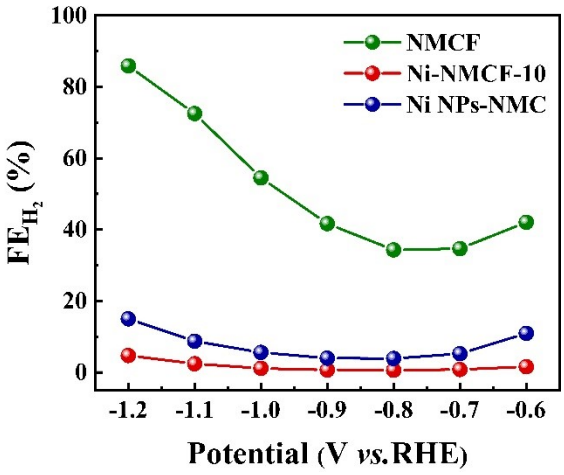

Figure S19. FE_{H2} of NMCF, Ni-NMCF-10, and Ni NPs-NMC catalysts in the H-type cell

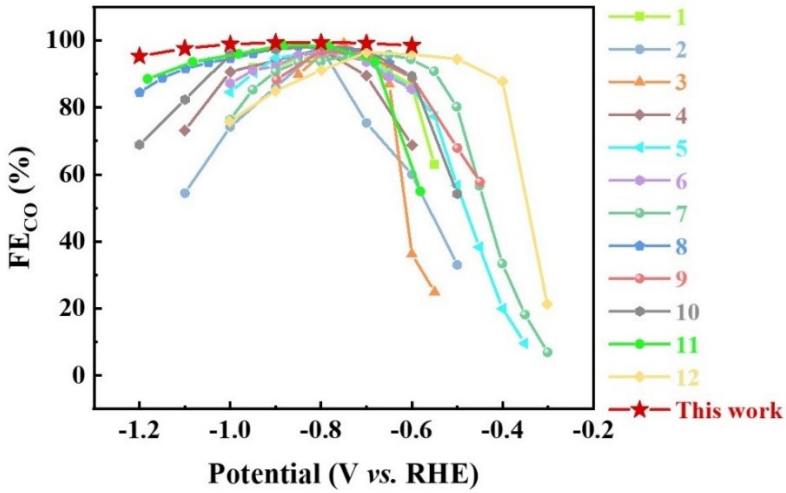

Figure S20. Comparisons of the potential range of our synthesized Ni-NMCF-10 catalyst with those Ni-N-C electrocatalysts reported in *Angewandte Chemie-International Edition* over the last 6 years (From 2019 to 2024). (*Angewandte Chemie-International Edition*[1-12])

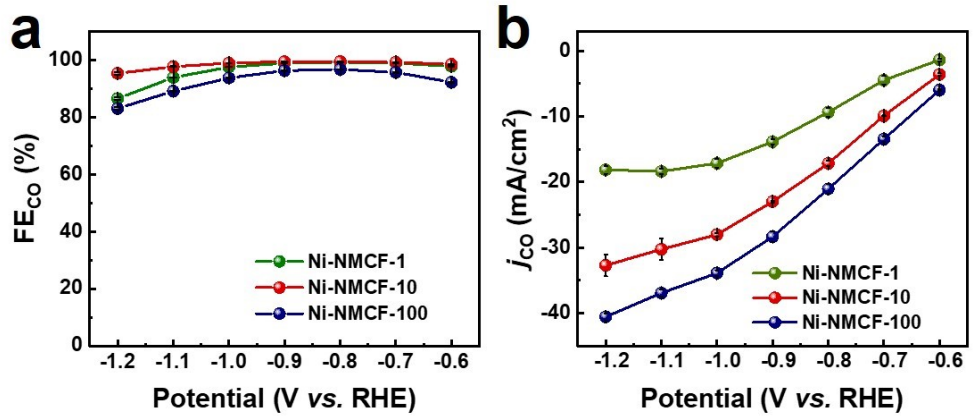

Figure S21. a) FE_{CO} and **b)** J_{CO} of Ni-NMCF-x catalysts in the H-type cell.

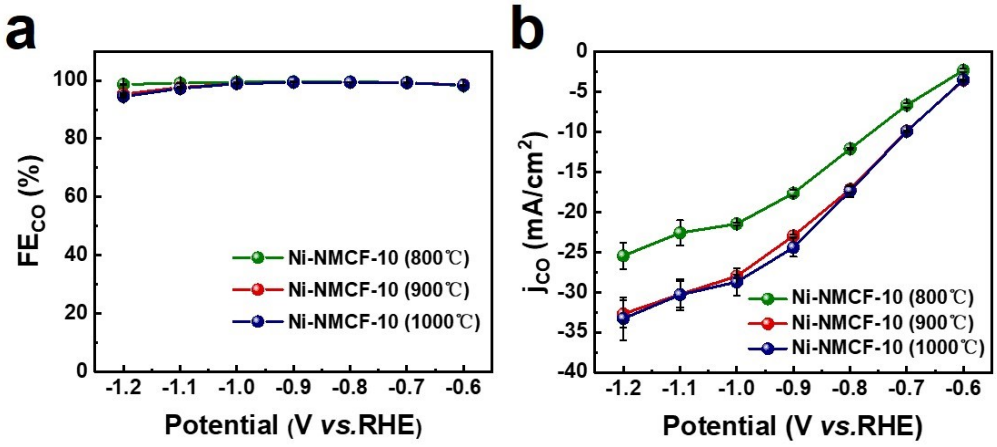

Figure S22. a) FE_{CO} and **b)** J_{CO} of Ni-NMCF-10 (T) catalysts in the H-type cell.

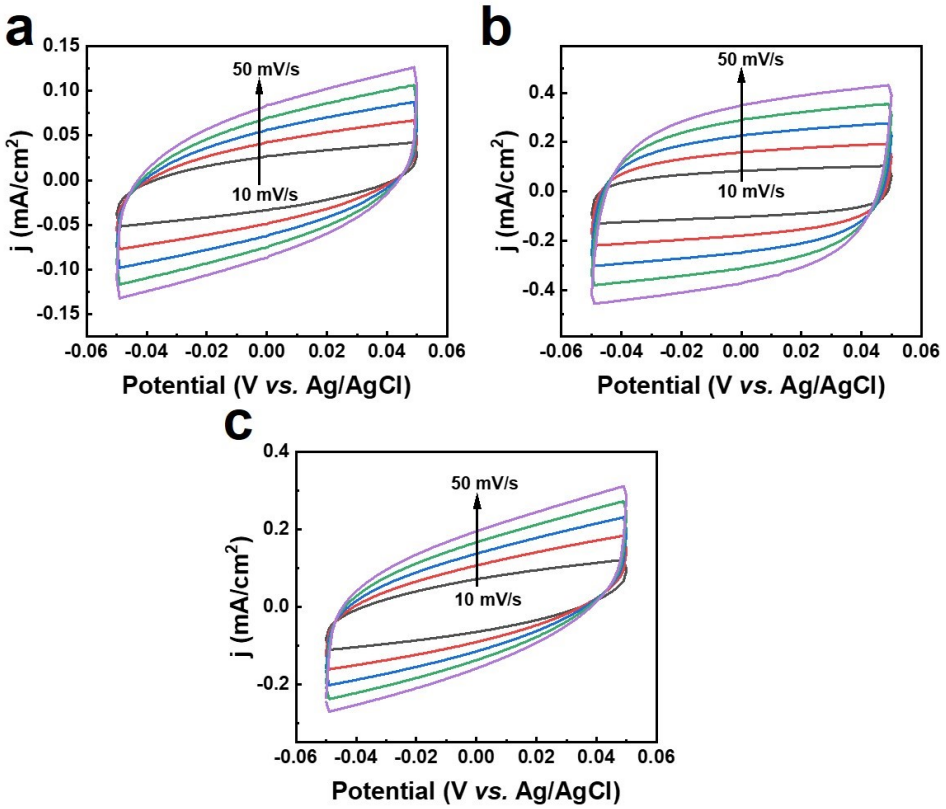

Figure S23. CV curves of **a)** NMCF, **b)** Ni-NMCF-10, and **c)** Ni NPs-NMC catalysts at different scan rates in a non-Faradaic region from -0.05 to 0.05 V in the CO_2-saturated 0.5 M $KHCO_3$.

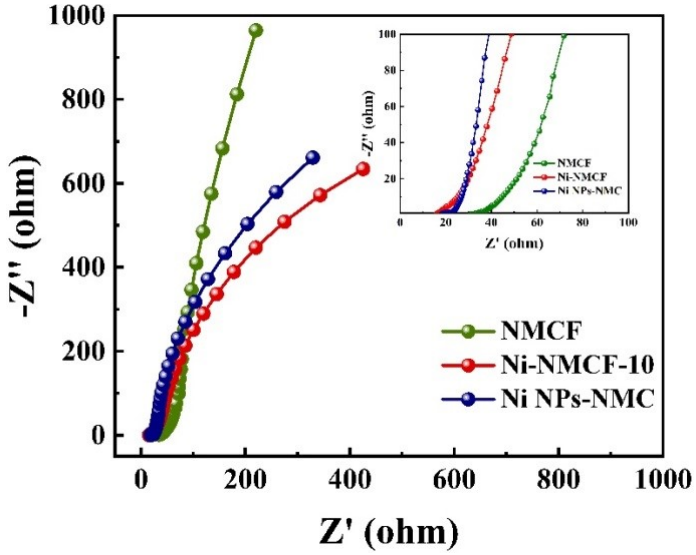

Figure S24. Nyquist plots of NMCF, Ni-NMCF-10, and Ni NPs-NMC catalysts.

Table S1. Contents of Ni species in our catalysts extracted from Inductively Coupled

Plasma Optical Emission Spectroscopy (ICP-OES) date.

Electrocatalysts	Ni (wt%)
Ni-NMCF-1	0.13
Ni-NMCF-10	0.32
Ni-NMCF-100	1.52

Table S2. Comparison of CO_2RR to CO performances of the Ni-NMCF-10 catalyst based on the previously reported Ni-N-C materials in H-type cell. (To compare the performance of our synthesized catalyst more objectively. We collected the recently reported work published in Angewandte Chemie-International Edition, Journal of the American Chemical Society, and Advanced Materials over the last 5 years (From 2019 to 2024))

Catalyst	FE_{max} (%)	E (V)[a]	E (FE_{CO} >90%) (mV)	Ref
Ni-NMCF-10	**99.4**	**-0.8**	**600[b]**	**This work**
Ni_1-N-C-50	94	-0.7	<300[c]	1
Ni_{SA}-N_2-C	98	-0.8	<200[c]	2
Ni_1-N/CNT	99	-0.75	150	3
Ni SAs	97.0	-0.80	<300[b]	4
Ni_1-N-C	96.8	-0.8	300	5
Ni-CNC-1000	96.6	-0.8	<400[c]	6
Ni-N_3-C	95.6	-0.65	450	7
NiPc-NiO_4	98.4	-0.85	450	8
NiNG-S	97	-0.8	<200[c]	9
CBNNiGd-700	99	-0.8	400	10
Ni_2–N_3C_4	98.9	-0.88	400	11
InNi DS/NC	96.7	-0.7	300	12
Ni-N_3-V	94	-0.8	200	13
Ni-CNT-CC	/	/	300	14
Ni/Fe-N-C	98	-0.7	400	15

Ni^{I}-NCNT@Ni_9Cu	97	-0.73	<200[c]	[16]
Ni-N_4-O/C	99.2	-0.9	600	[17]
Ni SAs	97	-0.8	<300[c]	[18]
Ni-SAC	93.8	-0.92	<100[c]	[19]
Ni-N_4-C	99	-0.81	400	[20]
Ni SAs/N-C	71.9	-0.9	0	[21]
Ni/Cu-N-C	97.7	-0.7	<700[c]	[22]
Fe_1-Ni_1-N-C	96.2	-0.5	<250[c]	[23]
$C_{250}Ph_{3.5}Ni$	/	/	1200	[24]
Ni-NC(AHP)	~100	-0.9	400	[25]
NiZn-N_6-C	99	-0.8	500	[26]

a: This value corresponds to the potential at the optimal CO Faraday efficiency

b: The FE_{CO} of >95% in a wide potential range from -0.65 to -1.45 V.

c: This value was obtained by measuring the chart of FE_{CO} versus potential in their manuscript.

Table S3. Comparison of the performances of the Ni-NMCF-10 catalyst based on the previously reported M-N-C materials for Zn-CO_2 batteries.

Catalyst	Catholyte	P_{max} ($mW \cdot cm^{-2}$)	FE (%)	Ref
Ni-NMCF-10	**1 M $KHCO_3$**	**2.4**	**98.7**	**This work**
CoPc/S-NHC	0.5 M $KHCO_3$	2.68	/	[27]
DNG-SAFe	1 M $KHCO_3$	3.33	86.5	[28]
Fe_1NC/S_1-1000	0.8 M $KHCO_3$	0.526	/	[29]
Cu-N_2/GN	0.5 M $KHCO_3$	0.6	64	[30]
CA/N-Ni	0.5 M $KHCO_3$	0.5	98	[31]
Ni-N_3-NCNFs	0.5 M $KHCO_3$	1.05	96	[32]
CoPc@DNHCS-8	0.8 M $KHCO_3$	1.02	94	[33]
Sn/NCNFs	0.5 M $KHCO_3$	1.38	97.6	[34]

Fe-N_4O-C/Gr	0.5 M $KHCO_3$	0.96	91	[35]
Zn/NC NSs	0.5 M $KHCO_3$	1.1	95	[36]
Ni-N_3-C	0.8 M $KHCO_3$	/	93	[7]
Co SAs@NCMF	1 M $KHCO_3$	0.61	/	[37]
Fe_1-Ni_1-N-C	0.8 M $KHCO_3$	/	93.4	[23]
NiFe-DASC	2 M KCl	0.89	90.6	[38]
Fe-P@NCPs	1 M $KHCO_3$	0.85	92	[39]
I-Ni SA/NHCRs	1 M $KHCO_3$	2.54	94.26	[40]
Ni@N-C	1 M $KHCO_3$	1.64	90	[41]

Reference:

1. M. Wen, N. Sun, L. Jiao, S. Q. Zang and H. L. Jiang, *Angewandte Chemie International Edition*, 2024, **136**, e202318338.
2. Y. N. Gong, L. Jiao, Y. Qian, C. Y. Pan, L. Zheng, X. Cai, B. Liu, S. H. Yu and H. L. Jiang, *Angewandte Chemie International Edition*, 2020, **132**, 2727-2731.
3. S. Jin, Y. Ni, Z. Hao, K. Zhang, Y. Lu, Z. Yan, Y. Wei, Y. R. Lu, T. S. Chan and J. Chen, *Angewandte Chemie International Edition*, 2020, **59**, 21885-21889.
4. Z. Li, D. He, X. Yan, S. Dai, S. Younan, Z. Ke, X. Pan, X. Xiao, H. Wu and J. Gu, *Angewandte Chemie International Edition*, 2020, **59**, 18572-18577.
5. L. Jiao, W. Yang, G. Wan, R. Zhang, X. Zheng, H. Zhou, S. H. Yu and H. L. Jiang, *Angewandte Chemie International Edition*, 2020, **59**, 20589-20595.
6. X. Cao, L. Zhao, B. Wulan, D. Tan, Q. Chen, J. Ma and J. Zhang, *Angewandte Chemie International Edition*, 2021, **61**, e202113918
7. Y. Zhang, L. Jiao, W. Yang, C. Xie and H. L. Jiang, *Angewandte Chemie International Edition*, 2021, **60**, 7607-7611.
8. J. D. Yi, D. H. Si, R. Xie, Q. Yin, M. D. Zhang, Q. Wu, G. L. Chai, Y. B. Huang and R. Cao, *Angewandte Chemie International Edition*, 2021, **60**, 17108-17114.
9. C. Jia, X. Tan, Y. Zhao, W. Ren, Y. Li, Z. Su, S. C. Smith and C. Zhao, *Angewandte Chemie International Edition*, 2021, **60**, 23342-23348.
10. W. Liu, P. Bai, S. Wei, C. Yang and L. Xu, *Angewandte Chemie International Edition*, 2022, **61**, e202201166.
11. Y. N. Gong, C. Y. Cao, W. J. Shi, J. H. Zhang, J. H. Deng, T. B. Lu and D. C. Zhong, *Angewandte Chemie International Edition*, 2022, **61**, e202215187.
12. Z. Fan, R. Luo, Y. Zhang, B. Zhang, P. Zhai, Y. Zhang, C. Wang, J. Gao, W. Zhou, L. Sun and J. Hou, *Angewandte Chemie International Edition*, 2023, **62**, e202216326.

13. X. Rong, H. J. Wang, X. L. Lu, R. Si and T. B. Lu, *Angewandte Chemie International Edition*, 2019, **59**, 1961-1965.
14. S. Liu, H. B. Yang, S. F. Hung, J. Ding, W. Cai, L. Liu, J. Gao, X. Li, X. Ren, Z. Kuang, Y. Huang, T. Zhang and B. Liu, *Angewandte Chemie International Edition*, 2019, **59**, 798-803.
15. W. Ren, X. Tan, W. Yang, C. Jia, S. Xu, K. Wang, S. C. Smith and C. Zhao, *Angewandte Chemie International Edition*, 2019, **58**, 6972-6976.
16. T. Zhang, X. Han, H. Yang, A. Han, E. Hu, Y. Li, X. q. Yang, L. Wang, J. Liu and B. Liu, *Angewandte Chemie International Edition*, 2020, **59**, 12055-12061.
17. X. Wang, Y. Wang, X. Sang, W. Zheng, S. Zhang, L. Shuai, B. Yang, Z. Li, J. Chen, L. Lei, N. M. Adli, M. K. H. Leung, M. Qiu, G. Wu and Y. Hou, *Angewandte Chemie International Edition*, 2021, **60**, 4192-4198.
18. Z. Li, D. He, X. Yan, S. Dai, S. Younan, Z. Ke, X. Pan, X. Xiao, H. Wu and J. Gu, *Angewandte Chemie International Edition*, 2020, **59**, 18572-18577.
19. W. Xie, H. Li, G. Cui, J. Li, Y. Song, S. Li, X. Zhang, J. Y. Lee, M. Shao and M. Wei, *Angewandte Chemie International Edition*, 2021, **60**, 7382-7388.
20. X. Li, W. Bi, M. Chen, Y. Sun, H. Ju, W. Yan, J. Zhu, X. Wu, W. Chu, C. Wu and Y. Xie, *Journal of the American Chemical Society*, 2017, **139**, 14889-14892.
21. C. Zhao, X. Dai, T. Yao, W. Chen, X. Wang, J. Wang, J. Yang, S. Wei, Y. Wu and Y. Li, *Journal of the American Chemical Society*, 2017, **139**, 8078-8081.
22. J. Zhu, M. Xiao, D. Ren, R. Gao, X. Liu, Z. Zhang, D. Luo, W. Xing, D. Su, A. Yu and Z. Chen, *Journal of the American Chemical Society*, 2022, **144**, 9661-9671.
23. L. Jiao, J. Zhu, Y. Zhang, W. Yang, S. Zhou, A. Li, C. Xie, X. Zheng, W. Zhou, S.-H. Yu and H.-L. Jiang, *Journal of the American Chemical Society*, 2021, **143**, 19417-19424.
24. D. Xi, J. Li, J. Low, K. Mao, R. Long, J. Li, Z. Dai, T. Shao, Y. Zhong, Y. Li, Z. Li, X. J. Loh, L. Song, E. Ye and Y. Xiong, *Advanced Materials*, 2021, **34**, 2104090.
25. Y. Li, S. L. Zhang, W. Cheng, Y. Chen, D. Luan, S. Gao and X. W. Lou, *Advanced Materials*, 2021, **34**, 2105204.
26. Y. Li, B. Wei, M. Zhu, J. Chen, Q. Jiang, B. Yang, Y. Hou, L. Lei, Z. Li, R. Zhang and Y. Lu, *Advanced Materials*, 2021, **33**, 2102212.
27. H. Wang, J. Zhu, X. Ren, Y. Tong and P. Chen, *Advanced Functional Materials*, 2024, **34**, 2312552.
28. W. Ni, Z. Liu, Y. Zhang, C. Ma, H. Deng, S. Zhang and S. Wang, *Advanced Materials*, 2020, **33**, 2003238.
29. T. Wang, X. Sang, W. Zheng, B. Yang, S. Yao, C. Lei, Z. Li, Q. He, J. Lu, L. Lei, L. Dai and Y. Hou, *Advanced Materials*, 2020, **32**, 2002430.
30. W. Zheng, J. Yang, H. Chen, Y. Hou, Q. Wang, M. Gu, F. He, Y. Xia, Z. Xia, Z. Li, B. Yang, L. Lei, C. Yuan, Q. He, M. Qiu and X. Feng, *Advanced Functional Materials*, 2019, **30**, 1907658.
31. Y. Zhang, X. Wang, S. Zheng, B. Yang, Z. Li, J. Lu, Q. Zhang, N. M. Adli, L.

Lei, G. Wu and Y. Hou, *Advanced Functional Materials*, 2021, **31**, 2104377.
32. W. Zheng, Y. Wang, L. Shuai, X. Wang, F. He, C. Lei, Z. Li, B. Yang, L. Lei, C. Yuan, M. Qiu, Y. Hou and X. Feng, *Advanced Functional Materials*, 2021, **31**, 2008146.
33. S. Gong, W. Wang, C. Zhang, M. Zhu, R. Lu, J. Ye, H. Yang, C. Wu, J. Liu, D. Rao, S. Shao and X. Lv, *Advanced Functional Materials*, 2022, **32**, 2110649.
34. X. Hu, Y. Liu, W. Cui, X. Yang, J. Li, S. Zheng, B. Yang, Z. Li, X. Sang, Y. Li, L. Lei and Y. Hou, *Advanced Functional Materials*, 2022, **33**, 2208781.
35. S. Chen, J. Chen, Y. Li, S. Tan, X. Liao, T. Zhao, K. Zhang, E. Hu, F. Cheng and H. Wang, *Advanced Functional Materials*, 2023, **33**, 2300801.
36. J. Chen, Z. Li, X. Wang, X. Sang, S. Zheng, S. Liu, B. Yang, Q. Zhang, L. Lei, L. Dai and Y. Hou, *Angewandte Chemie International Edition*, 2021, **61**, 202111683
37. Y. Zhao, Z. Pei, X. F. Lu, D. Luan, X. Wang and X. W. Lou, *Chem Catalysis*, 2022, **2**, 1480-1493.
38. Z. Zeng, L. Y. Gan, H. Bin Yang, X. Su, J. Gao, W. Liu, H. Matsumoto, J. Gong, J. Zhang, W. Cai, Z. Zhang, Y. Yan, B. Liu and P. Chen, *Nature Communications*, 2021, **12**, 4088.
39. S. Liu, L. Wang, H. Yang, S. Gao, Y. Liu, S. Zhang, Y. Chen, X. Liu and J. Luo, *Small*, 2022, **18**, 2104965.
40. S. Gong, S. Yang, W. Wang, R. Lu, H. Wang, X. Han, G. Wang, J. Xie, D. Rao, C. Wu, J. Liu, S. Shao and X. Lv, *Small*, 2023, **19**, 2207808.
41. F. Wang, G. Wang, P. Deng, Y. Chen, J. Li, D. Wu, Z. Wang, C. Wang, Y. Hua and X. Tian, *Small*, 2023, **19**, 2301128.